January 1, 2002

Climatology and storm time dependence ofnighttime thermospheric neutral winds over Millstone Hill

Bela G. Fejer, *Utah State University*
J. T. Emmert
D. P. Sipler

Climatology and storm time dependence of nighttime thermospheric neutral winds over Millstone Hill

B. G. Fejer and J. T. Emmert
Center for Atmospheric and Space Sciences, Utah State University, Logan, Utah, USA

D. P. Sipler
Haystack Observatory, Massachusetts Institute of Technology, Westford, Massachusetts, USA

Received 11 September 2001; revised 14 November 2001; accepted 14 November 2001; published 14 May 2002.

[1] We use 630.0 nm nightglow Fabry-Perot measurements over Millstone Hill from 1989–1999 to study the climatology and storm time dependence of the midlatitude thermospheric winds. Our quiet time wind patterns are consistent with results from earlier studies. We determine the perturbation winds by subtracting from each measurement the corresponding quiet time averages. The climatological zonal disturbance winds are largely independent of season and solar flux and show large early night westward and small late-night eastward winds similar to disturbance ion drifts. The meridional perturbation winds vary strongly with season and solar flux. When the solar flux is low, the winter and equinox average meridional winds change from equatorward to poleward at ~2200 LT, and the summer winds are equatorward throughout the night. The high solar flux meridional winds are poleward, with magnitudes increasing from dawn to dusk at all seasons. These disturbance winds patterns are in poor agreement with results from the empirical horizontal wind model, HWM-93. The zonal and meridional disturbance winds show very large variations relative to their average values. We have also studied the time-dependent response of the midlatitude thermospheric winds to enhanced magnetic activity. The early night westward winds build up to large amplitudes (about twice their climatological values) in ~6 hours; the late-night eastward winds are smaller and reach their peak values ~3 hours after the increase in magnetic activity. The storm time dependence of the meridional winds is considerably more complex than that of the zonal winds, and it varies with season and solar flux. Following enhanced magnetic activity, equatorward winds are observed at all local times and seasons, but the increase of their amplitudes with storm time is fastest in the late local time sector. Near midnight, and when the solar flux is low, the meridional winds reverse from equatorward to poleward ~6–10 hours after the increase in magnetic activity. This reversal is fastest (slowest) during December (June) solstice. At later local times, and for high solar flux conditions, the variation of the meridional disturbance winds is season independent. The observed storm time dependence partly explains the large variability of the disturbance winds. *INDEX TERMS:* 0358 Atmospheric Composition and Structure: Thermosphere—energy deposition; 2427 Ionosphere: Ionosphere/atmosphere interactions (0335); 2443 Ionosphere: Midlatitude ionosphere; *KEYWORDS:* midlatitude thermosphere, Fabry-Perot winds, disturbance thermospheric winds, ionosphere-thermosphere coupling

1. Introduction

[2] Extensive studies of midlatitude thermospheric winds have been carried out using ground-based ionosonde, incoherent scatter radar (ISR), and Fabry-Perot interferometer (FPI) measurements, in situ and remote sensing satellite data, and general circulation models [e.g., *Sipler et al.*, 1982; *Hernandez and Roble*, 1984; *Yagi and Dyson*, 1985; *Roble et al.*, 1987; *Crowley et al.*, 1989; *Buonsanto*, 1991; *Hedin et al.*, 1991; *Duboin and Lafeuille*, 1992; *Fuller-Rowell et al.*, 1994, 1996; *Titheridge*, 1995; *Burns et al.*, 1995; *Fesen et al.*, 1995; *Emery et al.*, 1999; *Kawamura et al.*, 2000]. These studies indicate quiet time midlatitude winds blowing away from diurnal pressure bulge and complex and highly variable patterns, with large and frequent wind surges associated with large-scale equatorward propagating disturbances, during geomagnetically disturbed times. An empirical climatological model of middle- and low-latitude thermospheric winds was presented by *Hedin et al.* [1996].

[3] The morphology of quiet time meridional thermospheric winds derived from Millstone Hill radar (42.6°N, 288.5°E, apex magnetic latitude 54°) measurements was studied initially by *Emery* [1978], *Babcock and Evans* [1979], and *Hagan* [1993]. Several subsequent studies have examined geomagnetic storm effects on the large-scale midlatitude ionospheric structure and dynamics, and on frictional heating, using Millstone Hill incoherent scatter radar and Fabry-Perot observations [e.g., *Buonsanto et al.*, 1990, 1992, 1999; *Hagan and Sipler*, 1991]. Recently, *Buonsanto and Witasse* [1999] used radar observations during 1984–1997 to update the climatologies of geomagnetically quiet and disturbed Millstone Hill *F* region ion drifts and meridional neutral winds during low and moderate solar flux conditions. These authors reported only very small geomagnetic effects on the climatological meridional neutral wind patterns, but they did not use data with $Kp > 5$, when there are often large errors in the calculation of the meridional radar winds due to gradients in the ion drifts.

0148-0227/02/2001JA000300

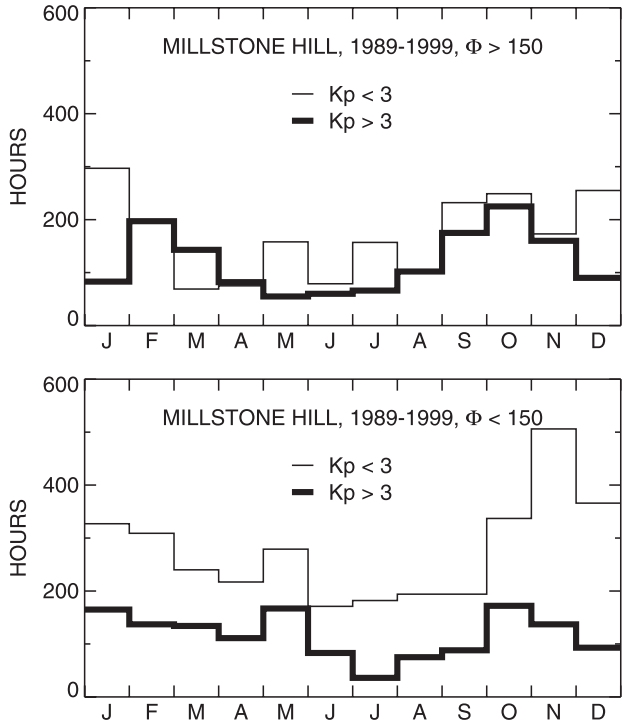

Figure 1. Yearly distributions of the number of hours of Millstone Hill Fabry-Perot observations used in this study. Here Φ denotes the decimetric solar flux index.

[4] Over the last decade a very large database of 630.0 nm nightglow Fabry-Perot observations has been collected at Millstone Hill by D. Sipler and coworkers. We use this extensive database to study in more detail the solar cycle and season-dependent climatology of the nighttime midlatitude thermospheric disturbance winds. We also present, for the first time, their storm time dependent response to geomagnetic disturbances using the methodology introduced by *Fejer and Scherliess* [1997]. This work complements the recent study of climatology and storm time dependence of midlatitude electrodynamic plasma drifts using Saint-Santin and Millstone Hill incoherent scatter radar data [*Scherliess et al.*, 2001].

[5] In sections 2 and 3.1 we first describe the experimental procedure for measuring Fabry-Perot thermospheric winds from Millstone Hill and then examine the local time and seasonal and solar cycle dependence of the nighttime winds during geomagnetically quiet times. Section 3.2 describes the climatology of the disturbance winds obtained by subtracting their solar cycle and season-dependent quiet wind values. Finally, we study the storm time dependence of these disturbance winds, which also varies strongly with local time, season, and solar activity.

2. Measurement Technique

[6] The Millstone Hill FPI wind measurements were described by *Sipler et al.* [1991] and *Buonsanto et al.* [1992]. The standard operating mode uses a vertical measurement and four measurements at an elevation angle of 30° at azimuths of 45°, 135°, 225°, and 315°. This set provides two orthogonal wind measurements at the same latitude to the north and south of the observatory. The winds above Millstone Hill are obtained by interpolating the measurements from the north and south (∼4° apart in latitude for a typical emission height of ∼280 km) and neglecting longitudinal gradients. The vertical wind is assumed to be negligible, and so the zenith measurements are used to determine the zero velocity reference. The uncertainties in the line-of-sight winds are determined statistically using the procedure described by *Hernandez* [1986], and instrumental drifts are monitored using a frequency stabilized laser. The cycle time depends on the strength of the nightglow signal. The interferometer takes data in a given direction until either a signal-to-noise ratio is achieved, or a time limit (∼10 min) is reached; the maximum total cycle time is ∼1 hour.

[7] Our Millstone Hill database consists of 8850 hours of wind observations covering ∼1150 nights from January 1989 and December 1999. These measurements have an average cycle time of ∼20 min, and average uncertainty of ∼25 m/s, and correspond to an average emission height between ∼250 and 280 km. Figure 1 shows the monthly distribution of the number of hours of measurements for two solar flux and geomagnetic activity levels. This database has the largest number of observations during December solstice and the smallest near June solstice, which is partly due to the longer periods of darkness during winter. The number of measurements during summer disturbed conditions is relatively small.

3. Results and Discussion

[8] In this section we initially examine the local time, season, and solar cycle dependent quiet time zonal and meridional Millstone Hill winds and compare them with results from the horizontal wind model, HWM-93 [*Hedin et al.*, 1996]. Our quiet time results are used primarily for determining the perturbation winds during geomagnetically active periods, and therefore they are not discussed in much detail. Sections 3.2 and 3.3 present the climatology of the disturbance winds and their storm time dependence.

3.1. Quiet Time Average Wind Patterns

[9] We have determined the nighttime seasonal- and solar-dependent average quiet time winds by averaging the data in sliding 2-hour bins when $Kp < 3$ for both the actual and two immediately preceding periods. Figure 2 presents these results for

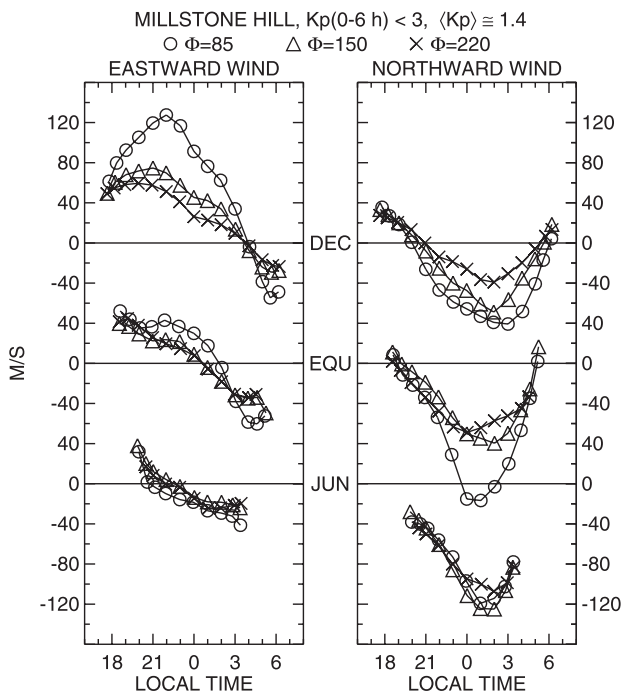

Figure 2. Local time, seasonal, and solar cycle dependence of quiet time *F* region winds over Millstone Hill. The low, moderate, and high solar flux patterns were obtained by binning the data for Φ < 105, 100–200, and >185.

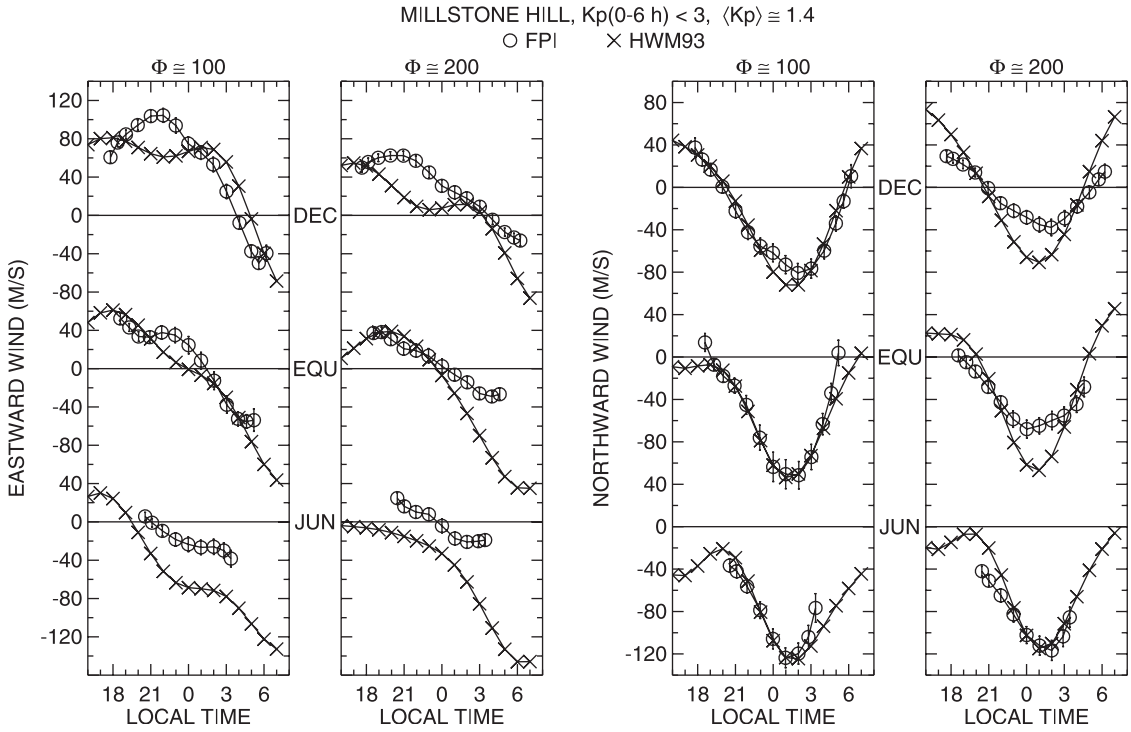

Figure 3. Comparison of Fabry-Perot and horizontal wind model, 1993 (HWM-93) winds for quiet time conditions.

December solstice (November–February), equinox (March–April and September–October), and June solstice (May–August) for low, moderate, and high decimetric solar flux conditions. We combined the data from the vernal and autumnal equinoxes since the corresponding average patterns are essentially identical, which is consistent with previous studies [e.g., *Duboin and Lafeuille*, 1992; *Hagan*, 1993]. These data correspond to an average $Kp \approx 1.4$. The standard errors of the mean, computed by dividing the standard deviations by the square roots of the number of nights in each bin, are of the order of 5–10 m/s.

[10] Figure 2 shows that the premidnight zonal winds vary from ~120 m/s eastward during December solstice low solar flux conditions to small eastward and westward values during the June solstice. Strong solar flux effects occur only during the December solstice. The postmidnight zonal winds are westward, have magnitudes between ~20 and 60 m/s, and do not change much with season and solar flux, except the crossover time from eastward to westward is earliest in June and latest in December. The meridional winds are predominantly equatorward for all seasons and have magnitudes between ~140 and 20 m/s, with smallest values during high solar flux periods. Solar activity dependence is again strongest during the December solstice and is virtually absent during June solstice. In summary, the seasonal and solar cycle dependence of horizontal thermospheric winds decreases significantly with the increase of ion drag.

[11] The meridional winds presented above are generally in good agreement with the Millstone Hill average radar winds presented by *Hagan* [1993] and *Buonsanto and Witasse* [1999], who used a much smaller number of observations. Our quiet time zonal and meridional winds are also consistent with the Fabry-Perot wind patterns over Fritz Peak (39.9°N, 105.5°W), as presented by *Hernandez and Roble* [1984, 1995]. The effects of EUV and high-latitude heating and ion drag on the meridional winds were discussed by *Hagan* [1993], who pointed out that the high-latitude circulation cell, driven by auroral processes, plays an important role in the variability of the thermospheric circulation over Millstone Hill even under magnetically quiet conditions. *Kawamura et al.* [2000] showed that the quiet time meridional wind patterns derived from Millstone Hill, Saint-Santin (46°N, 2.2°E), and the middle and upper atmosphere (MU) (34.9°N, 136.1°E) radar measurements are nearly identical for solar maximum, but not near solar minimum, when ion drag is smaller.

[12] Figure 3 shows the comparison of the nighttime Millstone Hill Fabry-Perot and HWM-93 model winds [*Hedin et al.*, 1996] for low and high solar flux quiet time conditions. The HWM winds were evaluated on days 0, 90, and 180 at a height of 250 km for the location of Millstone Hill (i.e., with longitudinal effects included) and for the same overall (seasonally averaged) flux and *Kp* values as the FPI data. (The HWM patterns evaluated at an altitude of 300 km give essentially identical results.) Figure 3 indicates that the FPI and the HWM zonal winds are eastward in the early nighttime period and turn to westward at later local times, but the late-night HWM westward winds are generally much larger than the Millstone Hill values. The FPI and the HWM meridional winds are in very good agreement for low solar flux conditions. For high solar flux conditions both models show smallest southward winds during December solstice but, except for June solstice, the HWM overestimates their peak amplitudes. These results reflect the fact that Millstone Hill solar minimum meridional winds derived from incoherent scatter radar measurements were used in the development of the HWM.

3.2. Average Disturbance Wind Patterns

[13] We determined the disturbance winds for $Kp > 3$ by subtracting the corresponding seasonal and solar cycle dependent average quiet time ($Kp < 3$ over the preceding 6 hours) values [e.g., *Fejer and Scherliess*, 1997]. These perturbation winds associated were averaged in 2-hour bins centered each hour from 1800 to 0600 LT. Figure 4 shows the seasonal and solar cycle dependence of these average disturbance winds for $\Delta Kp \approx 3$ over our average quiet time level ($Kp \approx 1.4$), and the variation of the season and solar flux averaged disturbance zonal drifts derived from incoherent scatter radar data. These average plasma drifts, which will be discussed later, have an average solar flux index $\Phi \approx 130$

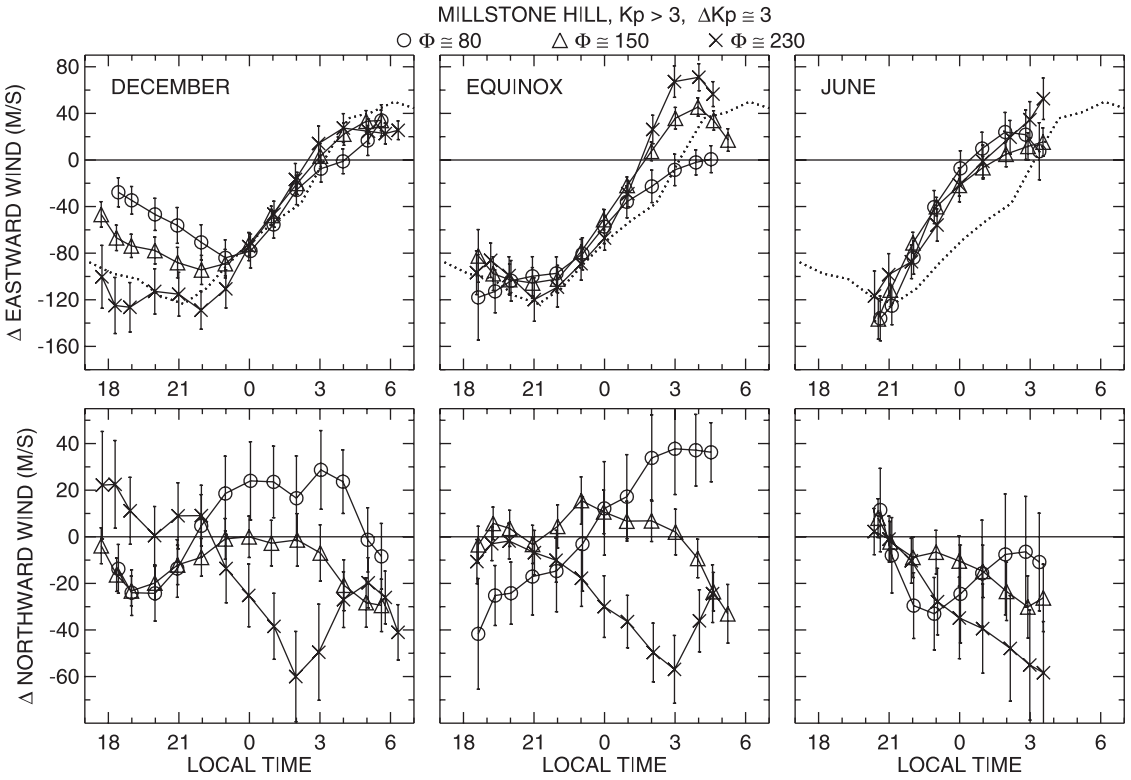

Figure 4. Average disturbance wind patterns for low, moderate, and high solar flux conditions; the error bars denote the standard errors of the means. The dotted curve denotes the season and solar flux averaged zonal disturbance drift pattern derived from incoherent scatter radar data.

but are largely season and solar flux independent. The meridional winds have noticeably larger errors of the mean than the zonal winds due to their much stronger seasonal solar cycle and, as we will see later, storm time variability. The zonal perturbation winds data are westward with magnitudes up to ~130 m/s during the early night period; the late-night winds are eastward and have smaller magnitudes. Solar cycle effects are strongest during December solstice, when there is a large increase of the westward winds from solar minimum to solar maximum. The meridional perturbation winds show largest seasonal dependence near solar minimum when they are predominantly northward and southward during December and June solstice, respectively. Near solar maximum the meridional disturbance wind patterns are nearly season independent and have largest southward winds at ~0300 LT.

[14] The *Kp* dependence of the disturbance winds is illustrated in more detail in Figure 5. In this case the seasonally averaged perturbation zonal winds show very large westward and smaller eastward perturbations in the early and late-night periods, respectively. The transition from westward to eastward perturbations occurs slightly earlier with increasing magnetic activity. Figure 4 indicates that near solar minimum the December solstice and equinoctial meridional perturbation wind patterns are nearly identical and that the high solar flux disturbance winds are largely season independent. Therefore in the bottom and middle right-hand panels in Figure 5 we show the average meridional disturbance winds from September through April for low and moderate solar fluxes, and in the top panel we show the seasonally averaged solar maximum wind patterns. The *Kp* dependence of the meridional winds is clearly more complex than that of the zonal winds, as a result of their stronger seasonal solar cycle and as will be shown later, especially due to their storm time variations. The magnitudes of the late-night southward perturbation winds near solar maximum can reach 60–70 m/s for $\Delta Kp \approx 4$. These large southward perturbations are most likely the climatological signatures of

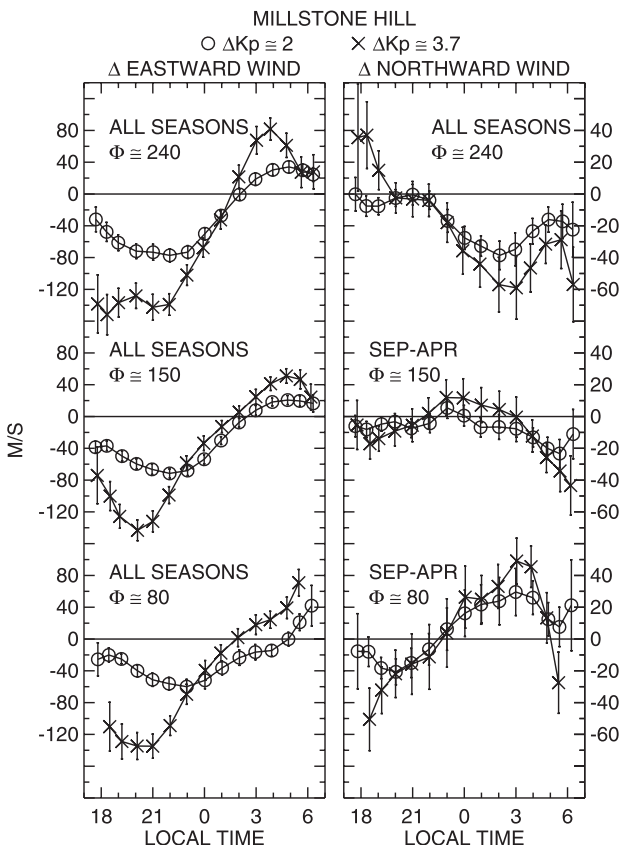

Figure 5. Zonal and meridional disturbance wind patterns for two levels of geomagnetic activity ($3 \leq Kp \leq 4$, and $Kp > 4$).

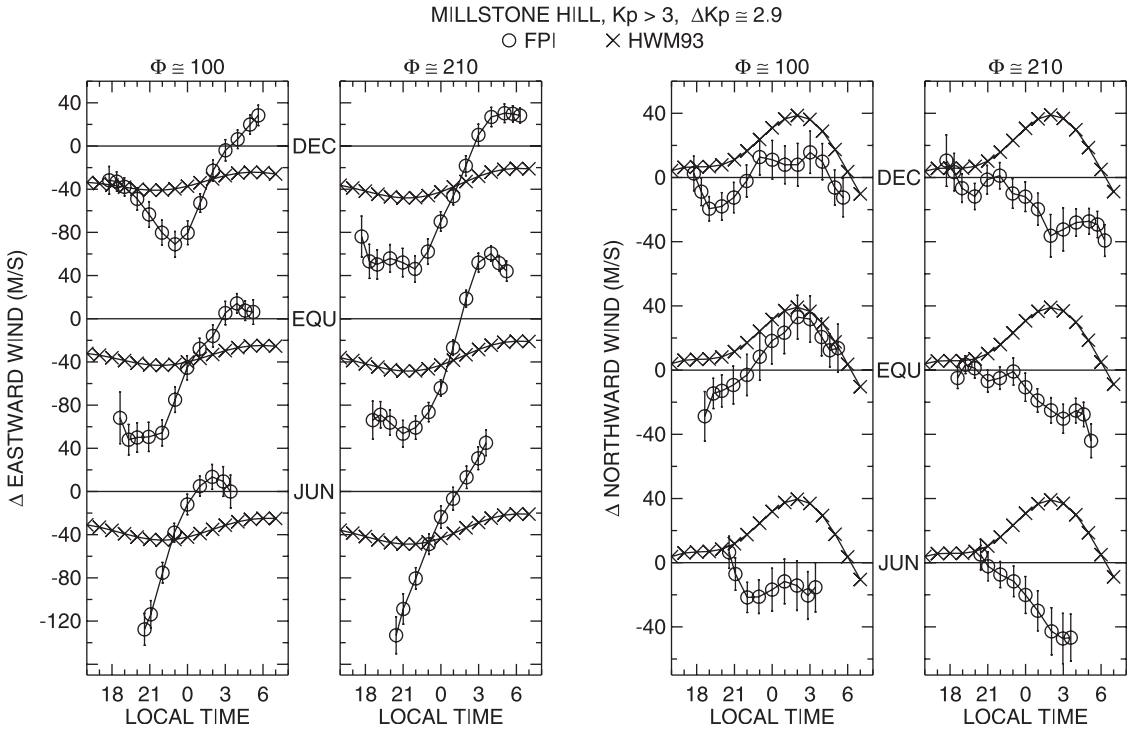

Figure 6. Millstone Hill Fabry-Perot and HWM-93 disturbance wind patterns.

equatorward surges in the meridional neutral wind, which is a common feature of the disturbed postmidnight thermosphere above Millstone Hill [e.g., *Buonsanto et al.*, 1990; *Buonsanto*, 1995].

[15] *Buonsanto and Witasse* [1999] reported that during low and moderate solar flux conditions, there are only very minor magnetic activity effects on the climatology of the Millstone Hill radar meridional winds. However, as mentioned earlier, these authors did not use data with $Kp > 5$. Figures 2 and 5 indicate that for the range of solar flux and Kp values considered by Buonsanto and Witasse, the meridional disturbance winds are generally small compared with their quiet time values. Our climatological meridional disturbance wind patterns are in good agreement with Saint-Santin nighttime radar wind results presented by *Duboin and Lafeuille* [1992], particularly for solar minimum conditions.

[16] We have seen that the Millstone Hill FPI and HWM-93 quiet time nighttime horizontal wind patterns are generally consistent. We calculated the solar maximum and minimum HWM disturbance winds for $\Delta Kp \approx 3$ using the same procedure as in our data analysis, i.e., subtracting the $Kp = 1.4$ winds from the $Kp = 4.3$ values. Figure 6 compares these HWM disturbance winds and our empirical results. In this case the low and high solar flux Fabry-Perot winds were obtained by averaging the data for $\Phi < 150$ and $\Phi \geq 150$, respectively. The HWM zonal disturbance winds are westward throughout the night and have no seasonal and solar cycle dependence. This model significantly underestimates the early night large westward perturbation winds and does not reproduce the observed reversal to eastward in the postmidnight sector. The HWM meridional disturbance winds are almost always poleward with a peak around 0200 LT. These results are in fair agreement with the Millstone Hill solar minimum perturbation winds during the December solstice and equinox, but they are completely inconsistent with our June solstice solar minimum and with our solar maximum results for all seasons. As mentioned earlier, this empirical model used Millstone Hill solar minimum meridional wind data derived from incoherent scatter radar measurements. *Emmert et al.* [2001] showed that the daytime HWM-93 disturbance winds are in very poor agreement with Wind Imaging Interferometer (WINDII) measurements from UARS at middle and low latitudes. These results indicate that this model does not provide a realistic representation of the climatology of thermospheric winds during disturbed conditions.

[17] The above results describe the climatology of the Millstone Hill disturbance winds. However, the thermospheric winds during disturbed conditions show variability around their average values. Figure 7 illustrates this variability as a function of the Kp index for the evening zonal winds and for the late-night solar maximum meridional winds. The average westward disturbance winds are very small for $Kp < 3$ but increase sharply for $Kp > 5$, reaching values of ~300 m/s for $Kp \approx 8$. Very large westward perturbation winds in the evening midlatitude thermosphere during strongly active conditions were studied by *Reddy and Mayr* [1998] using DE-2 satellite measurements. These perturbation winds were shown to be highly correlated with strongly enhanced magnetospheric convection, which can extend equatorward of Millstone Hill during strongly disturbed periods. Figure 7 also indicates the increase of the variability of the evening westward winds with magnetic activity. The meridional disturbance winds have standard deviations larger than their climatological averages. The variability of these winds is largest in the premidnight sector and for lower solar conditions.

[18] In section 3.3 we will show that the very large variability of the meridional winds is, to a large extent, due to their strong storm time dependence. Of course, there is also significant variability on both the zonal and meridional winds as a result of temporal and spatial changes in the enhanced high-latitude convection and energy deposition, which affect the large-scale thermospheric circulation and generate equatorward-traveling atmospheric waves.

3.3. Storm Time Dependent Disturbance Winds

[19] Storm time dependent studies require the use of higher time resolution magnetic activity indices than the Kp index used in our climatological averages. Storm time electric field studies [e.g., *Fejer and Scherliess*, 1997; *Scherliess et al.*, 2001] have often used

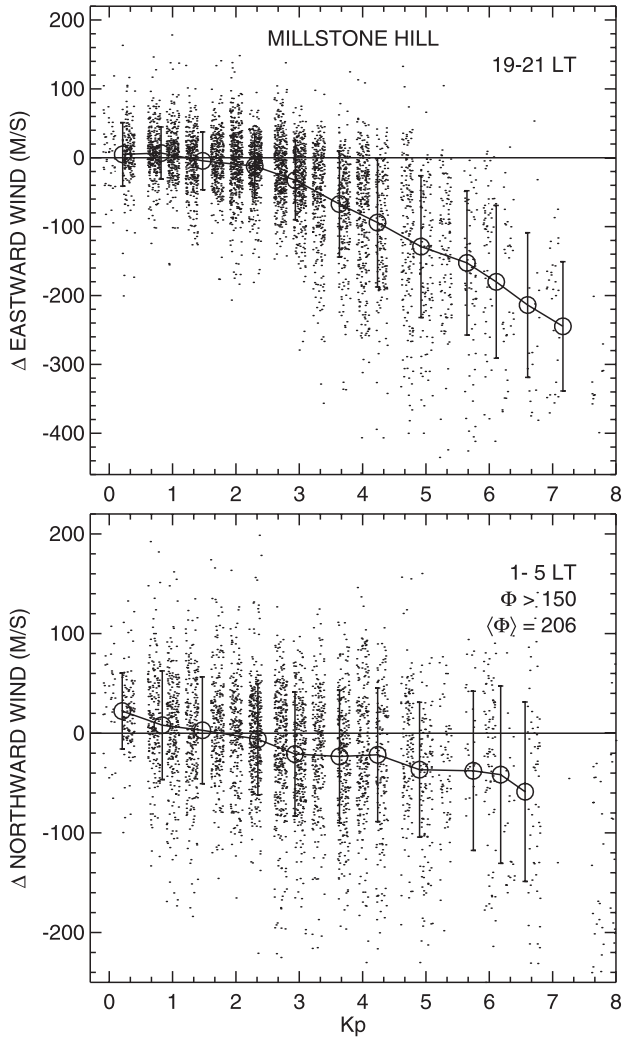

Figure 7. Scatterplots of the early night zonal (all fluxes), and late-night meridional high solar flux meridional winds as a function of the *Kp* index. The average values and standard deviations are also shown.

the *AE* index as the magnetic activity parameter, but this index is not available for the entire period of our Fabry-Perot measurements. Therefore in the present study we use the 15-min Polar Cap (PC) index, which was introduced in 1988 as a measure of geomagnetic disturbances and has been shown to be well correlated with various solar wind parameters and geomagnetic indices. In particular, the PC index is highly correlated with the *AE* indices [*Vennerstrom et al.*, 1991; *Vassiliadis et al.*, 1996; *Takalo and Timonen*, 1998] and also provides a good proxy for the hemispheric Joule heating rate [*Chun et al.*, 1999].

[20] Since the zonal disturbance winds do not change much with season and solar flux, we have combined these data to determine their storm time response. Figure 8 shows, in the top panel, an idealized change in the PC index by ~2 units, which corresponds to an increase from an average $Kp \approx 1.8-4.2$. We define the storm time $t = 0$ as corresponding to the time when the PC index reaches one half of its average storm time value, which occurs ~1 hour after the steady increase of the index above its extended quiet value. The bottom panels present the local time variations of the disturbance zonal winds at the storm times shown in the top panel, obtained using a superposed epoch analysis [e.g., *Burns and Killeen*, 1992; *Scherliess et al.*, 2001]. In Figures 8–10 we define the storm onsets when the PC index was >1.8 ($Kp \approx 2.8$). Therefore the disturbance levels correspond to averages of the different PC indices >1.8, with the upper bound values slightly adjusted to give about the same averages at the different storm times.

[21] Figure 8 shows that following the increase in the PC index, the zonal perturbation winds are westward from about sunset up to ~0200 LT and eastward, with smaller amplitudes, later at night. These storm time patterns are quite similar to the climatological wind patterns shown in Figure 4. The early night westward disturbance winds increase for ~8 hours during the June solstice and for ~10–12 hours during equinox and the December solstice, but the amplitudes of the late-night eastward winds are largely unchanged after 3 hours of increased activity. The peak westward winds are smallest during the December solstice, which is consistent with the climatological averages and also with the smaller average Joule heating rates (calculated using the formulae from *Chun et al.* [1999]) compared to the June solstice and equinox. The peak westward winds at storm time t_3 (~120–200 m/s) are significantly larger than the moderate flux climatological values (~90–120 m/s) shown in Figure 5, even though the latter correspond to a higher level of magnetic activity. Of course, it is important to remember that the climatological averages depend on the average length of the storms and that somewhat different values are obtained when using the *Kp* or PC indices. After the decrease in magnetic activity, as indicated by the drop of the PC index, the perturbation wind pattern shifts to later local times as their magnitudes decrease with storm time. The disturbance winds largely vanish ~6–12 hours after the time of sudden geomagnetic quieting.

[22] The zonal perturbation wind patterns shown in Figure 8 closely resemble the disturbance zonal ion drift pattern shown in

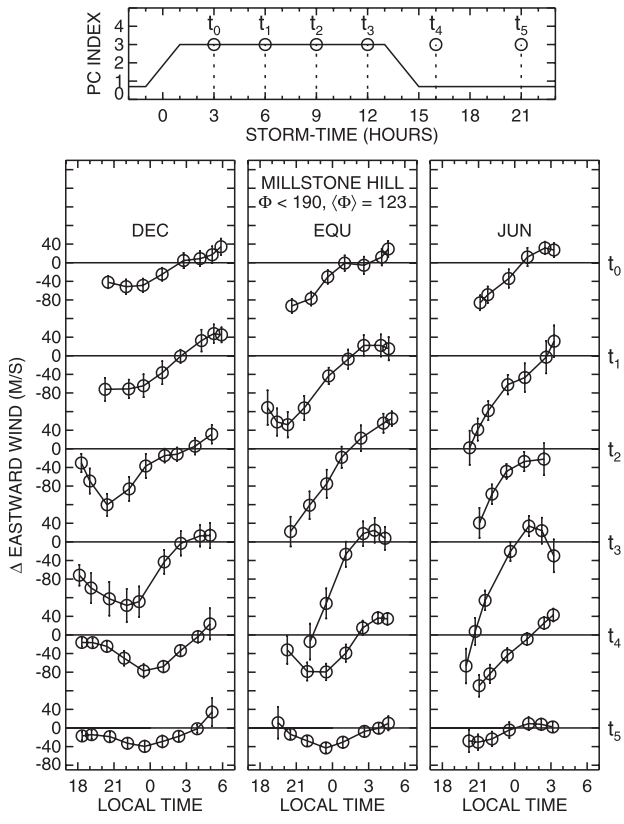

Figure 8. (top) Idealized variation of the PC index and (bottom) average zonal disturbance winds over Millstone Hill for the conditions and storm times shown in the top panel. The scatter bars denote the standard errors of the means.

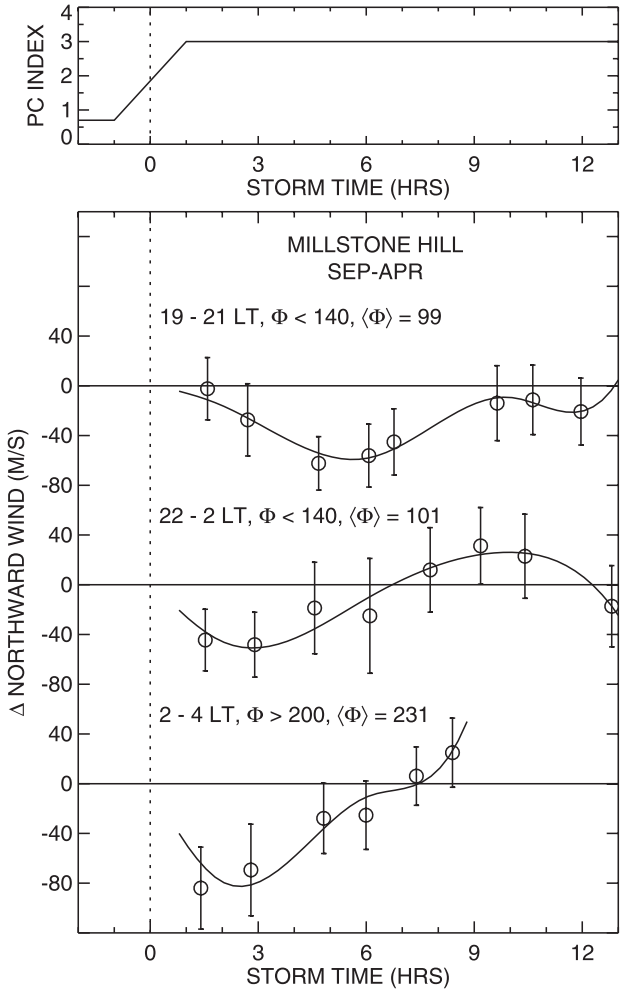

Figure 9. Storm time dependence of the September–April average disturbance meridional winds over Millstone Hill during the early night, midnight, and late local time sectors. The scatter bars denote the standard errors of the means.

Figure 4 and also the storm time dependent perturbation ion drifts derived by *Scherliess et al.* [2001]. This is expected considering the close coupling between the convection-driven neutral and the ionized gas motions. Thermospheric disturbance neutral winds can also be driven by enhanced Joule heating in the auroral zone [e.g., *Blanc and Richmond*, 1980; *Emery et al.*, 1999], which should produce enhanced westward nighttime winds at middle- and low-latitudes, with largest magnitudes near the longitudes of the magnetic poles. The HWM zonal disturbance winds shown in Figure 6 are all westward, probably dynamo winds. However, because of the proximity of Millstone Hill to the sources of thermospheric disturbances, it is difficult in a statistical study to separate the effects of enhanced convection from dynamo wind effects, especially in the premidnight sector, where they are both westward. However, the close similarity of the disturbance winds and ion drifts, as shown in Figure 4, clearly suggests that these disturbance winds are dominated by convection effects.

[23] The variations of the meridional winds with storm time are considerably more complex than those of the zonal winds, and they are also more difficult to parameterize due to the strong seasonal and solar cycle effects on these disturbance winds. Therefore for this wind component it is not meaningful to combine the data from all seasons and different solar flux values. We have seen in Figure 4 that the equinox and December solstice meridional disturbance wind patterns are quite similar during low solar flux early night hours and also during late-night high solar flux conditions. Figure 9 presents a superposed epoch analysis of these meridional winds following a sudden increase in the PC index by ~2.3 units, which corresponds to $\Delta Kp \approx 2.5$. We do not show our low solar flux late-night results that were based on a smaller number of measurements. Since there is a well-established relation between onset of auroral activity and the generation of equatorward traveling gravity waves [e.g., *Hocke and Schlegel*, 1996], our definition of storm time underestimates the response time of our thermospheric winds. Figure 9 shows that in the early night period the equatorward disturbance winds build up for ~6 hours to a peak value of ~60 m/s (about twice the average climatological value) and then appears to decrease to zero during the following 6 hours. Near midnight, equatorward disturbance winds build up significantly faster, reaching ~50 m/s in 3 hours, and then turn poleward between ~7 and 11 hours after the increase in magnetic activity, with a peak value of ~30 m/s. The late-night high solar flux winds have larger peak amplitudes (~80 m/s) but also reverse ~7 hours after the onset of geomagnetic activity. The peak amplitude of these late-night equatorward winds increases with solar activity and is ~40 m/s for an average solar flux index of ~120. However, the reversal time from equatorward to northward winds remains essentially unchanged.

[24] For low levels of solar activity our database of observations near midnight is large enough to examine the seasonal dependence of the storm time response of the meridional winds. This is shown in Figure 10, again for ΔPC index by ~2.3 units ($\Delta Kp \approx 2.5$). In this case we have verified that the average local time does not change much with storm time. The storm time coverage is shortest during the December solstice due to the smaller number of long-lasting storms in our database during this season. Similar patterns are also obtained using data between 2200 and 0200 LT for slightly higher solar flux values. These data indicate that the average

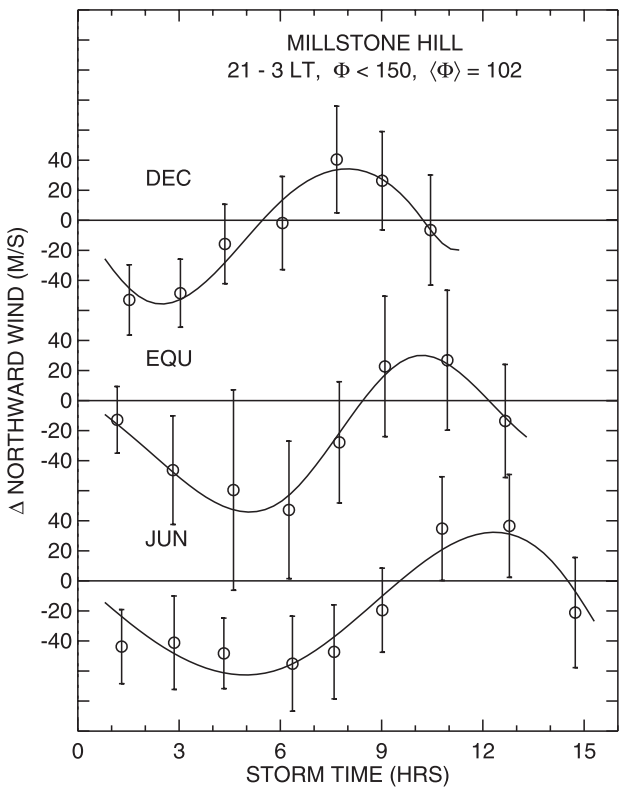

Figure 10. Seasonal and storm time dependence of the moderate flux meridional disturbance winds in the midnight sector. The scatter bars denote the standard errors of the means.

lifetime of the equatorward meridional wind surges near midnight is strongly season dependent. The reversal of the disturbance winds from equatorward to poleward winds occurs at earliest storm times during December solstice and latest for June solstice, with equinoctial reversal time somewhere in between. For storm times smaller than ~11 hours the December solstice data hours of storm time exhibit large equatorward and poleward winds but averages out to near zero, which is consistent with the climatological average near midnight for this season, shown in Figure 4. This also suggests that close to midnight the variability of the meridional winds is largest during December solstice moderate solar flux conditions. The storm time variations described above partly account for the large departures of the meridional disturbance winds from their climatological averages. For high solar activity levels the reversal of the meridional disturbance winds from poleward to equatorward near midnight is independent of season, and it occurs ~6–7 hours after the increase in the PC index.

[25] Strong equatorward wind surges at midlatitude stations during storms periods have been the subject of several studies [e.g., *Hernandez et al.*, 1980; *Yagi and Dyson*, 1985; *Buonsanto et al.*, 1990, 1992, 1999; *Buonsanto*, 1995; *Emery et al.*, 1999]. They are observed regularly during postmidnight storm periods and result primarily from pressure gradients set up by high-latitude Joule heating and ion drag, although Coriolis effects also seem to be important [*Forbes and Roble*, 1990; *Hagan and Sipler*, 1991]. The equatorward wind surges are associated with gravity waves which propagate with horizontal velocities between ~400 and 1000 m/s [*Hocke and Schlegel*, 1996]. *Emery et al.* [1999] reported significant gravity waves with phase speeds of ~700 m/s (22°/h) observed in the neutral temperature and wind fields during the 2–11 November 1993 storm period. These fast-traveling waves reach the equator in ~3 hours.

[26] Our storm time analysis indicates large equatorward winds following sudden increases in magnetic activity over the entire nighttime period and for all seasons, with largest amplitudes in the late-night sector, which is consistent with earlier studies. These disturbance winds are mostly driven by Joule and particle heating generated high-latitude pressure gradients and ion drag effects associated with magnetospheric convection. The time constant for ion drag effects (the inverse of the ion neutral collision frequency) can vary from <30 min to a few hours [e.g., *Buonsanto*, 1995]. It is difficult to sort out the relative importance of these processes using our single-site data. There are also significant equatorward wind perturbations near midnight during low solar flux periods. These perturbations occur at earliest and latest storm times during December and June solstice, respectively. When the solar flux is high, the reversal time of the midnight perturbation winds from equatorward to poleward is season independent, and it occurs ~5–6 hours after the sudden increase of geomagnetic activity. These measurements, however, clearly suggest the importance of wind sources equatorward of Millstone Hill. Significant gradients in the midlatitude wind field have been observed by several authors, suggesting the existence of wind circulation cells. *Hernandez et al.* [1982] pointed out that enhanced poleward and westward winds to the south and west of the Fritz Peak Observatory could be due to hemispheric differences in the thermospheric energy input, equatorward heating by neutral hydrogen, and an increased midnight equatorial temperature bulge.

[27] Since the meridional disturbance winds are strongly dependent on solar flux, season, and storm time, the parameterization of their response following sudden magnetic quieting is considerably more complex than that of their response to rapidly enhanced activity. Furthermore, studies using general circulation models indicate that long duration energy injection into the high-latitude ionosphere is effective in generating a meridional disturbance circulation, whereas short-duration injection preferentially generates atmospheric gravity waves [e.g., *Fujiwara et al.*, 1996]. Analysis of the temporal evolution of our meridional disturbance winds following a sudden decrease of magnetic activity indicates complex oscillatory meridional patterns which appear to die out ~6 hours after magnetic quieting.

4. Conclusions

[28] We have shown that very extensive measurements using the Millstone Hill Fabry-Perot interferometer have revealed a considerably detailed picture of the climatology of the midlatitude nighttime thermospheric neutral winds during geomagnetically quiet and active times. During the December solstice and equinox the quiet time zonal winds are eastward from dusk up to ~0300 LT and westward at later local times. The summer zonal winds are mostly westward. The quiet time meridional winds are equatorward from about dusk to dawn and have largest magnitudes during low solar flux conditions. These results are in fair agreement with the quiet time winds from HWM-93.

[29] The zonal disturbance winds are westward with large amplitudes in the early night sector and are eastward with smaller magnitudes in the late-night sector. These zonal disturbance winds are largely season and solar cycle independent, and they closely follow the pattern of the disturbance zonal ion drifts. The meridional perturbation winds are strongly dependent on season and solar flux. During low solar flux periods the December solstice and equinoctial meridional winds are equatorward at early night hours and poleward at later local times; the summer meridional winds are systematically equatorward. The high solar flux meridional winds are increasingly southward with increasing local time and do not change much with season. These perturbation wind patterns are in poor agreement with results from HWM-93. The disturbance winds show very large variability relative to their climatological values.

[30] We have studied the storm time dependence of the perturbation winds following a sudden increase in the high latitude currents as measured by the PC index. The westward disturbance winds increase in magnitude for ~6 hours following a step function increase in the PC index, whereas the later night eastward winds reach their peak values in ~3 hours. The zonal perturbation winds largely vanish ~6–12 hours after sudden magnetic quieting. The temporal response of the meridional perturbation winds to magnetic activity is strongly season and solar cycle dependent. For short storm times, meridional perturbation winds are equatorward at all local times. During the December solstice and equinox the equatorward perturbation winds build up faster with increasing local time and solar flux. The low solar flux perturbation winds near midnight reverse from equatorward to poleward earliest (latest) in storm time during winter (summer). For higher solar flux conditions and later local times the reversal from equatorward to poleward winds occurs ~6 hours after the step function increase in magnetic activity, independent of season. The strong storm time variation of the meridional perturbation winds partly explains their large departures from the climatological averages, particularly during low solar flux periods.

[31] **Acknowledgments.** This work was supported by the Aeronomy Program, Division of Atmospheric Sciences of the National Science Foundation through grant ATM-0004380.

[32] Janet G. Luhmann thanks Barbara A. Emery and Seiji Kawamura for their assistance in evaluating this paper.

References

Babcock, R. R., and J. V. Evans, Seasonal and solar cycle variations in the thermospheric circulation observed over Millstone Hill, *J. Geophys. Res.*, *84*, 7348–7352, 1979.

Blanc, M., and A. D. Richmond, The ionospheric disturbance dynamo, *J. Geophys. Res.*, *85*, 1669–1688, 1980.

Buonsanto, M. J., Neutral winds in the thermosphere at midlatitudes over a full solar cycle: A tidal decomposition, *J. Geophys. Res.*, *96*, 3711–3724, 1991.

Buonsanto, M. J., Millstone Hill incoherent scatter *F* region observations

during the disturbances of June 1991, *J. Geophys. Res.*, *100*, 5743–5755, 1995.

Buonsanto, M. J., and O. G. Witasse, An updated climatology of thermospheric winds and *F* region ion drifts over Millstone Hill, *J. Geophys. Res.*, *104*, 24,675–24,687, 1999.

Buonsanto, M. J., J. C. Foster, A. D. Galasso, D. P. Sipler, and J. M. Holt, Neutral winds and thermosphere/ionosphere coupling and energetics during the geomagnetic disturbances of March 6–10, 1989, *J. Geophys. Res.*, *95*, 21,033–21,050, 1990.

Buonsanto, M. J., J. C. Foster, and D. P. Sipler, Observations from Millstone Hill during the geomagnetic disturbance of March and April 1990, *J. Geophys. Res.*, *97*, 1225–1234, 1992.

Buonsanto, M. J., S. A. Gonzalez, G. Lu, B. W. Reinisch, and J. P. Thayer, Coordinated incoherent scatter radar study of the January 1997 storm, *J. Geophys. Res.*, *104*, 24,625–24,637, 1999.

Burns, A. G., and T. L. Killeen, The equatorial neutral thermospheric response to geomagnetic forcing, *Geophys. Res. Lett.*, *19*, 977–980, 1992.

Burns, A. G., T. L. Killeen, W. Deng, G. R. Carignan, and R. G. Roble, Geomagnetic storm effects in the low- to mid-latitude upper thermosphere, *J. Geophys. Res.*, *100*, 14,673–14,692, 1995.

Chun, F. K., D. L. Knipp, M. G. McHarg, G. Lu, B. A. Emery, S. Vennerstrom, and O. A. Troshichev, Polar cap index as a proxy for hemispheric Joule heating, *Geophys. Res. Lett.*, *26*, 1101–1104, 1999.

Crowley, G., B. A. Emery, R. G. Roble, H. C. Carlson, and D. J. Knipp, Thermospheric dynamics during September 18–19, 1984, 2, Validation of the NCAR thermospheric general circulation model, *J. Geophys. Res.*, *94*, 16,945–16,959, 1989.

Duboin, M. L., and M. Lafeuille, Thermospheric dynamics above Saint-Santin: Statistical study of the data set, *J. Geophys. Res.*, *97*, 8661–8671, 1992.

Emery, B. A., Neutral thermospheric winds derived above Millstone Hill, 2, Seasonal wind variations, *J. Geophys. Res.*, *83*, 5704–5716, 1978.

Emery, B. A., C. Lathuillere, P. G. Richards, R. G. Roble, M. J. Buonsanto, D. J. Knipp, P. Wilkinson, D. P. Sipler, and R. Niciejewski, Time dependent thermospheric neutral response to the 2–11 November 1993 storm period, *J. Atmos. Sol. Terr. Phys.*, *61*, 329–350, 1999.

Emmert, J. T., B. G. Fejer, C. G. Fesen, G. G. Shepherd, and B. H. Solheim, Climatology of middle- and low-latitude daytime *F* region disturbance neutral winds measured by Wind Imaging interferometer (WINDII), *J. Geophys. Res.*, *107*, 24,701–24,710, 2001.

Fejer, B. G., and L. Scherliess, Empirical models of storm time equatorial zonal electric fields, *J. Geophys. Res.*, *102*, 24,047–24,056, 1997.

Fesen, C. G., R. G. Roble, and M.-L. Duboin, Simulations of seasonal and geomagnetic activity effects at Saint-Santin, *J. Geophys. Res.*, *100*, 21,397–21,407, 1995.

Forbes, J. M., and R. G. Roble, Thermosphere-ionosphere coupling: An experiment in interactive modeling, *J. Geophys. Res.*, *95*, 201–208, 1990.

Fujiwara, H., S. Maeda, H. Fukunishi, T. J. Fuller-Rowell, and D. S. Evans, Global variations of thermospheric winds and temperatures caused by substorm energy injection, *J. Geophys. Res.*, *101*, 225–240, 1996.

Fuller-Rowell, T. J., M. V. Codrescu, R. J. Moffet, and S. Quegan, Response of the thermosphere and ionosphere to geomagnetic storms, *J. Geophys. Res.*, *99*, 3893–3914, 1994.

Fuller-Rowell, T. J., M. V. Codrescu, H. Rishbeth, R. J. Moffet, and S. Quegan, On the seasonal response of the ionosphere and thermosphere to geomagnetic storms, *J. Geophys. Res.*, *101*, 2343–2354, 1996.

Hagan, M. E., Quiet time upper thermospheric winds over Millstone Hill between 1984 and 1990, *J. Geophys. Res.*, *98*, 3731–3739, 1993.

Hagan, M. E., and D. P. Sipler, Combined incoherent scatter radar and Fabry-Perot interferometer measurements of frictional heating effects over Millstone Hill during March 7-10, 1989, *J. Geophys. Res.*, *96*, 289–296, 1991.

Hedin, A. E., et al., Revised global model of thermospheric winds using satellite and ground-based observations, *J. Geophys. Res.*, *96*, 7657–7688, 1991.

Hedin, A. E., et al., Empirical wind model for the upper, middle, and lower thermosphere, *J. Atmos. Terr. Phys.*, *58*, 1421–1447, 1996.

Hernandez, G., *Fabry-Perot Interferometers*, Cambridge Univ. Press., New York, 1986.

Hernandez, G., and R. G. Roble, The geomagnetic quiet nighttime thermospheric wind pattern over Fritz Peak Observatory during solar minimum and maximum, *J. Geophys. Res.*, *89*, 327–337, 1984.

Hernandez, G., and R. G. Roble, Thermospheric nighttime neutral wind temperature and winds over Fritz Peak Observatory: Observed and calculated solar cycle variation, *J. Geophys. Res.*, *100*, 14,647–14,659, 1995.

Hernandez, G., R. G. Roble, and J. H. Allen, Midlatitude thermospheric winds and their relationship to the auroral electrojet activity index, *Geophys. Res. Lett.*, *7*, 677–680, 1980.

Hernandez, G., R. G. Roble, E. C. Ridley, and J. H. Allen, Thermospheric response observed over Fritz Peak, Colorado, during two large geomagnetic storms near solar maximum, *J. Geophys. Res.*, *87*, 9181–9192, 1982.

Hocke, K., and K. Schlegel, A review of atmospheric gravity waves and traveling ionospheric disturbances: 1982-1995, *Ann. Geophys.*, *14*, 917–940, 1996.

Kawamura, S., Y. Otsuka, S.-R. Zhang, S. Fukao, and W. L. Oliver, A climatology of middle and upper atmosphere radar observations of thermospheric winds, *J. Geophys. Res.*, *105*, 12,777–12,788, 2000.

Reddy, C. A., and H. G. Mayr, Storm time penetration to low latitudes of magnetospheric-ionospheric convection and convection-driven thermospheric winds, *Geophys. Res. Lett.*, *25*, 3075–3078, 1998.

Roble, R. J., J. M. Forbes, and F. A. Marcos, Thermospheric dynamics during the March 22, 1979 magnetic storm, 1, Model simulation, *J. Geophys. Res.*, *92*, 6045–6068, 1987.

Scherliess, L., B. G. Fejer, J. Holt, L. Goncharenko, C. Armory-Mazaudier, and M. J. Buonsanto, Radar studies of midlatitude ionospheric plasma drifts, *J. Geophys. Res.*, *106*, 1771–1783, 2001.

Sipler, D. P., B. B. Luokkala, and M. A. Biondi, Fabry-Perot determinations of mid-latitude *F*-region neutral winds and temperatures from 1975 to 1979, *Planet. Space Sci.*, *20*, 1025–1032, 1982.

Sipler, D. P., M. E. Hagan, M. E. Zipf, and M. A. Biondi, Combined optical and radar wind measurements in the *F* region over Millstone Hill, *J. Geophys. Res.*, *96*, 21,255–21,262, 1991.

Takalo, J., and J. Timonen, Comparison of the dynamics of the AU and PC indices, *Geophys. Res. Lett.*, *25*, 2101–2104, 1998.

Titheridge, J. E., Winds in the ionosphere—A review, *J. Atmos. Sol. Terr. Phys.*, *57*, 1681–1714, 1995.

Vassiliadis, D., V. Angelopoulos, D. N. Baker, and A. J. Klimas, The relation between the northern polar cap and auroral electrojet indices in the wintertime, *Geophys. Res. Lett.*, *23*, 2781–2784, 1996.

Vennerstrom, S., E. Friis-Christensen, O. A. Troschichev, and V. G. Anderson, Comparison between the polar cap index PC and the auroral electrojet indices AE, AL, and AU, *J. Geophys. Res.*, *96*, 101–113, 1991.

Yagi, T., and P. L. Dyson, The response of the mid-latitude thermospheric wind to magnetic activity, *Planet. Space Sci.*, *33*, 461–467, 1985.

J. T. Emmert and B. G. Fejer, Center for Atmospheric and Space Sciences, Utah State University, Logan, UT 84222-4405, USA. (emmert@cc.usu.edu; bfejer@cc.usu.edu)

D. P. Sipler, Haystack Observatory, Massachusetts Institute of Technology, Westford, MA 01886, USA. (dsipler@haystack.mit.edu)